communications physics

Article

https://doi.org/10.1038/s42005-024-01570-4

Demonstration of a Josephson vortex-based memory cell with microwave energy-efficient readout

Check for updates

Dmitrii S. Kalashnikov[1,2] ✉, Vsevolod I. Ruzhitskiy[2,3,4], Andrey G. Shishkin[1,2,3], Igor A. Golovchanskiy[1], Mikhail Yu. Kupriyanov[2,4], Igor I. Soloviev[2,3,4], Dimitri Roditchev[5] & Vasily S. Stolyarov[1,2,3] ✉

The ongoing progress of superconducting logic systems with Josephson junctions as base elements requires the development of compatible cryogenic memory. Long enough junctions subject to magnetic field host quantum phase 2π-singularities—Josephson vortices. Here, we report the realization of the superconducting memory cell whose state is encoded by the number of present Josephson vortices. By integrating the junction into a coplanar resonator and by applying a microwave excitation well below the critical current, we are able to control the state of the system in an energy-efficient and non-destructive manner. The memory effect arises due to the presence of the natural edge barrier for Josephson vortices. The performance of the device is evaluated, and the routes for creating scalable cryogenic memories directly compatible with superconducting microwave technologies are discussed.

Superconducting electronics is expected to outperform semiconductor technologies in terms of speed and energy efficiency in a variety of applications, including certain media processing tasks, cryptography, artificial intelligence, digital and quantum computing[1]. Recent efforts in the field led to realization of digital logic[2–7], quantum computers[8–14], neuromorphic systems[15–21], among many others. Compatible cryogenic memory is critical for the self-sustainability of these devices. Current implementations of superconducting memories use superconducting loops involving Josephson junctions (JJs)[22–25], hybrid superconductor/ferromagnet structures[26–31], superconductor/ferroelectric elements[32], and also Abrikosov vortices[33,34] which are magnetic flux quanta inside a superconductor.

In a recent theoretical paper[35] the authors proposed using Josephson vortices (JVs) for the information storage. These vortices appear in a so-called long JJ, when their length becomes larger than the Josephson penetration depth, λ_J. In general, fundamentals of electrodynamics and JV dynamics in long JJs are well understood[36,37]. For instance, elongation of JJs leads to modification of the supercurrent-field characteristics[38–41], while the propagation of JVs in biased long junctions can result in self-excitation of plasmon-like resonant modes coupled to the JVs[42]. In addition, JVs can couple to the external DC and microwave electromagnetic fields[43–46], which facilitates the control over the state of JVs and allows even to address its quantum dynamics[45]. Importantly, all static and dynamic phenomena in long JJs can be well captured by the sin-Gordon equation, which is well demonstrated in references mentioned above.

The principle of operation of JV-based memory takes advantage of the hysteretic behavior of a long JJ in an external magnetic field, which was briefly described already in 1965 by Brian Josephson[47] and studied in detail in several theoretical works[40,41]. In fact, similarly to Bean-Livingston[48–52] or geometrical[53] barriers for Abrikosov vortex penetration into a superconductor, there exists a barrier for JV entry a long ($\gg \lambda_J$) JJ; these barriers depend on junction geometry, used materials, etc. Their presence resulted, for instance, in the resistance oscillations in a magnetic field observed in layered superconductors containing intrinsic JJs[54,55]. Thus at the same magnetic field, a long JJ can be found not only in the lowest energy state but also in one of metastable states with different number of JVs inside, depending on the history of the system.

In this paper, we demonstrate the realization of a superconducting memory element based on bi-stability of long JJ. The controlled switching between the zero-JV state of the junction and its one-JV state is obtained by finite time changing of an external magnetic field directed perpendicularly to the device plane. This process will be denoted as a magnetic field or a current pulse further in the text. The state of the Josephson junction is read

[1]Center for Advanced Mesoscience and Nanotechnology, Moscow Institute of Physics and Technology, Dolgoprudny 141700, Russia. [2]National University of Science and Technology MISIS, Moscow 119049, Russia. [3]Dukhov Research Institute of Automatics (VNIIA), Moscow 127030, Russia. [4]Skobeltsyn Institute of Nuclear Physics, Lomonosov Moscow State University, Moscow 119991, Russia. [5]Laboratoire de Physique et d'Etudes des Materiaux, ESPCI-Paris, PSL Research University, CNRS, Sorbonne University, Paris 75005, France. ✉e-mail: kalashnikov.ds@phystech.edu; stolyarov.vs@phystech.edu

by the microwave current. This operation is possible due the dependence of the JJ impedance on the number of JVs present inside the junction. The sensitivity of the detection is enhanced by integrating the JJ in the microwave coplanar resonator. Importantly, the state of the JJ is identified (read) even at currents much lower than its critical current I_c. The use of sub-critical currents has several advantages as compared to read operations requiring the measurements of I_c: enhanced energy efficiency of the memory and non-destruction of its initial state. We analyze the performance of the memory element and discuss the possibilities for improving it based on the results of the developed theoretical model.

Results

Microwave response and the junction state

In the present work, four identical planar $L = 1.9$ μm long Superconductor/Normal metal/Superconductor (SNS) Josephson junctions (see inset in Fig. 1a) were studied. From additional DC current experiments, we determined the value of their critical Josephson current $I_c \approx 940$ μA and estimated the Josephson penetration length to $\lambda_J = 245$ nm. Consequently, $L \approx 7.6\,\lambda_J$, and thus the junction is long enough to accommodate several Josephson vortices. The junctions were located in the central line of the $\lambda/4$ coplanar resonators near their ends. An example of the JJ integrated into a 4.5 GHz resonator is presented in Fig. 1a. The resonators were notch-connected to the common coplanar waveguide used for both, the microwave excitation and the transmission measurement. The resonators have different resonant frequencies enabling addressing them separately. At a fixed input power P and magnetic field B, the frequency f of the microwave signal is swept and the scattering parameter $S_{21}(f)$ is registered. It should be emphasized that the measurements were provided at low input power $P = -90$ dBm, corresponding to AC currents flowing through the junction ~4 μA, which is by two orders of magnitude lower than I_c. This enables us to consider the JJ as a linear system. Notice that the JJ never reached the normal state during measurements. Also, the excitation frequency range, $f = 3$–5 GHz, was chosen well below the critical (Josephson) frequency $f_c = 2eV_c/h \approx 70$ GHz.

Figure 1b shows two dips in $S_{21}(f)$ measured at zero-field (blue curve) and at 0.26 mT (red curve). They are due to the absorption of the microwave by the resonator. The curves are Lorentz-shaped and can be described by the resonant frequency, f_r, the internal quality factor, Q_i, of the resonator, including the losses in the resonator itself and in the JJ, and the coupling quality factor, Q_c, linked to the energy leak from the resonator to the measurement coplanar line. These parameters can be obtained by fitting the experimental data by the expression[56]:

$$S_{21}(f) = 1 - \frac{Q_l/Q_c}{1 + 2iQ_l(f/f_r - 1)}, \tag{1}$$

where $Q_l = (Q_i^{-1} + \mathrm{Re}\{Q_c^{-1}\})^{-1}$ is the total quality factor.

Figure 1c is a color plot of $S_{21}(f)$ as a function of rising magnetic field $0 \rightarrow 0.65$ mT. It demonstrates the existence of 5 field windows characterized by a smooth evolution $S_{21}(f, B)$. Each window is associated with a fixed number, from 0 to 4, of JV inside the junction. The regions are separated by sharp transitions (denoted by vertical dashed lines). Figure 1 d, e details the magnetic field evolution of the resonant frequency $f_r(B)$ and of the inverse internal quality factor $Q_i^{-1}(B)$. These parameters are directly related to the complex impedance $Z_L = R_L + iX_L$ of the Josephson junction that adds to the impedance $Z_0 \gg Z_L$ of the resonator itself and detunes the resonant frequency and the quality factor[57]:

$$f_r = f_r^0\left(1 - \frac{2}{\pi}\frac{X_L}{Z_0}\right); \quad \frac{1}{Q_i} = \frac{1}{Q_i^0} + \frac{4}{\pi}\frac{R_L}{Z_0}, \tag{2}$$

where f_r^0 and Q_i^0 are the resonant frequency and the quality factor of the resonator itself, while R_L and X_L represent, respectively, the effective resistance and reactance of the JJ. Table 1 summarizes the essential parameters of the resonator extracted from the data for different numbers N of JVs present.

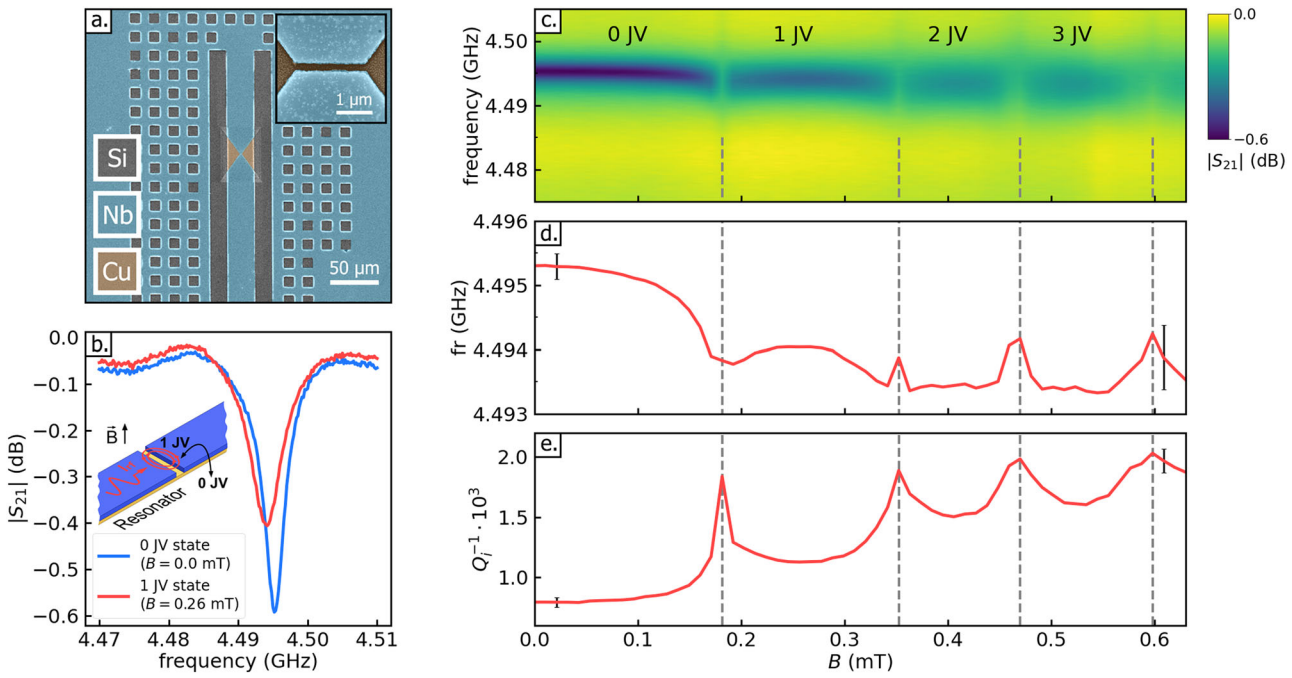

Fig. 1 | Microwave detection of Josephson vortex (JV) inside a long Superconductor/Normal metal/Superconductor junction. a Artificially colored image (top view) of a 4.5 GHz Nb/Cu/Si microwave resonator with a 2 μm long planar Nb-Cu-Nb junction implemented in the central line (the total length of the resonator is about 7 mm). Inset: a zoom on the junction area. The images were obtained using a scanning electron microscope; **b** resonance modes of the resonator observed as sharp dips in the scattering parameter $S_{21}(f)$ signal at zero-applied magnetic field (blue curve) and at $B = 0.26$ mT (red curve). Inset: a scheme of microwave measurements of JVs; **c** color plot of $S_{21}(f, B)$. Vertical dashed lines delimit regions with different fixed numbers of JVs present in the junction; **d** magnetic field dependence of the resonance frequency and, **e** of the inverse internal quality factor. The data in (**d**) and (**e**) are extracted from $S_{21}(f, B)$.

Table 1 | Parameters of the resonator and the Josephson junction (JJ) with a different number of Josephson vortices (JVs)

JJ state, N	f_r, GHz	$Q_i^{-1} \cdot 10^3$	$R_L(N) - R_L(0)$, mΩ	$X_L(N) - X_L(0)$, mΩ
0 JV	4.4953	0.79	0	0
1 JV	4.4940	1.13	13	22
2 JV	4.4934	1.50	28	33
3 JV	4.4934	1.60	32	33

Resonance frequency f_r, inverse internal quality factor Q_i^{-1} and variations of the real R_L and imaginary X_L parts of the complex impedance Z_L for different numbers N of JVs in the JJ extracted from data in Fig. 1c using the formulas (1) and (2).

It becomes immediately clear that the $R_L(N)$ increases with N. Obtained dependence qualitatively coincides with the calculated curve in the work[58] where the surface impedance of the infinite Josephson contact in the external magnetic field was investigated. The reason for this additional dissipation is the forced motion of JVs inside the JJ under microwave excitation. Indeed, since $f \ll f_c$, and the amplitude of microwave current is well below I_c, the excitation can be seen as a source of a tiny oscillatory Lorentz force that slightly shakes the JV around its equilibrium position inside the junction. The minimum of dissipation expectantly occurs when no JV are present. At $N = 1$, the dissipation parameter R_L increases by 13 mΩ; the fact that this is by an order of magnitude lower than the normal JJ resistance $R_N = 150$ mΩ is consistent with the expected low amplitude of JV forced motion due to excitation. At $N = 2$, it increases by 28 mΩ. This doubling of dissipation is simply explained by two JVs moving back and forth along the junctions, instead of one. However, adding one more JV does not triple the dissipation. A possible reason could be related to the limited size of the junction, $L \approx 7.6\,\lambda_J$, that can only accept 3–4 JVs at maximum. As N increases, JVs start to interact, reducing the effect of microwave excitation per vortex. Note also, that for $N > 2$ the precision of determining R_L and X_L drops significantly and cannot be considered as reliable anymore.

We can now understand the global oscillatory evolution of $Q_i^{-1}(B)$ presented in Fig. 1e. For each N, there exists a field value corresponding to the minimum energy and to the most stable equilibrium for JVs in the junction (that was shown in Fig. 3 in the work[40]); it is zero for $N = 0$, 0.26 mT for $N = 1$, 0.41 mT for $N = 2$, etc. At these fields, the amplitude of JV forced motion and the related dissipation R_L are lowest, and $Q_i^{-1}(B)$ experiences local minima. When the magnetic field deviates from these values, the potential in which evolve JVs flattens; this results in an increase of the forced motion amplitude and, consequently, of the dissipation; Q_i^{-1} raises. Close to the field values corresponding to the transitions $N \rightarrow N \pm 1$ (denoted by vertical dashed lines in Fig. 1) the potential flattens, JV motion amplitude is the highest, the dissipation is strongest, resulting in peaks in Q_i^{-1}. It has to be noted that a similar behavior of JVs in long JJ was observed in works[59–62] where the JJ was coupled to a mechanic resonator represented by the oscillating magnetic cantilever of the MFM microscope. Similarly to microwave excitation, the cantilever excites the motion of the JV inside the junction and probes the corresponding energy dissipation. The authors showed that the highest energy dissipation occurs when individual JVs enter or exit the junction.

Vortex hysteresis effect

For the implementation of a memory element, the key effect is the hysteresis of the system in a magnetic field near $N \rightarrow N \pm 1$. In this work, using subcritical microwave currents, we were able to clearly observe the hysteresis effect in our Josephson contacts. Figure 2a, b shows the magnetic field dependencies of $S_{21}(f)$ measured for the opposite directions of the magnetic field sweeps around zero. The obtained patterns are globally symmetric and coincide, except for the two regions, -0.27 mT $< B < -0.21$ mT and $+0.21$ mT $< B < +0.27$ mT, where $0 \rightleftarrows \pm 1$ transitions occur. In these regions, both the transition field and $S_{21}(f, B)$ evolution depend on the field sweep direction. Precisely, the resonance frequency lowers smoothly when

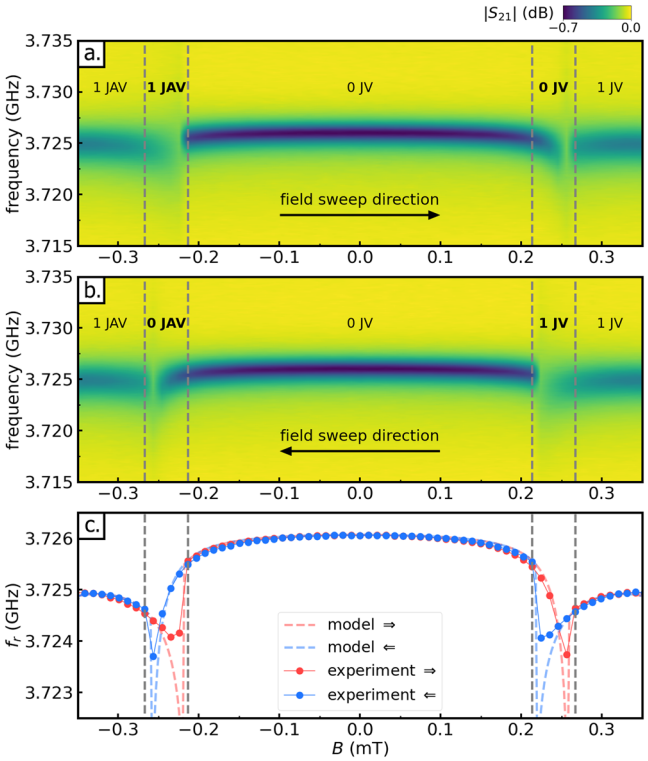

Fig. 2 | Hysteresis in $N \rightleftarrows N + 1$ Josephson vortex transitions. Images (**a**) and (**b**) are color plots of the scattering parameter $S_{21}(f, B)$ recorded from a 3.73 GHz resonator at opposite field sweep directions (marked by arrows). The hysteresis regions are delimited by vertical dashed lines. The numbers in the images (**a**) and (**b**) indicate the number of Josephson vortices (JV) and antivortices (JAV); **c** variations of the resonant frequency f_r as the field is swept from negative to positive values (red dots) and back (blue dots). Color dashed lines are corresponding numerical fits.

the field approaches the transition field from the current state but jumps abruptly to the next state. This dynamics always coincides with the direction of the field sweep and therefore it is not a simple displacement of the pattern in a magnetic field. This eliminates the possibility that the observed hysteresis is created elsewhere, by the solenoid, for instance, and not in the Josephson junction. Despite the fact that the hysteresis region is rather narrow, it is perfectly reproducible.

Our numerical simulations of the system's behavior robustly support the experimental data and working hypotheses and enable a deeper insight in the microscopic processes inside the junction. The details about the numerical model can be found in the Methods section and Supplementary Note 1. Our model successfully reproduced the entry and exit of JVs, the hysteresis effect and the observed transition asymmetry in $f_r(B)$. Precisely, the model curves (blue and red dashed lines in Fig. 2c) nicely follow the experimental data points and reproduce a smooth decrease in the resonant frequency when exiting the current state, and then a sharp dynamics when entering the following state. During modeling this process we considered a planar JJ of a geometry reproducing the experimentally studied one, as presented in Fig. 3a. The critical current distribution in the junction was taken constant inside the junction and exponentially decaying outside, Fig. 3b. Though in the model, the resonant frequency drop was found deeper than in the experiment, down to $f = 3.721$ GHz. This occurs because the model does not take into account the losses in the resonator, a non-uniform focusing of the magnetic field due to the flat geometry or a JV shaking by microwave excitation. Figure 3c shows the distribution of the magnetic field inside the Josephson junction obtained from the model in an external magnetic field equal to $B_0 = 0.22$ mT, which corresponds to the hysteresis region. This result shows that at the same field, the JJ can indeed be in two different stable states, characterized by the number (0 or 1) of JVs inside. The

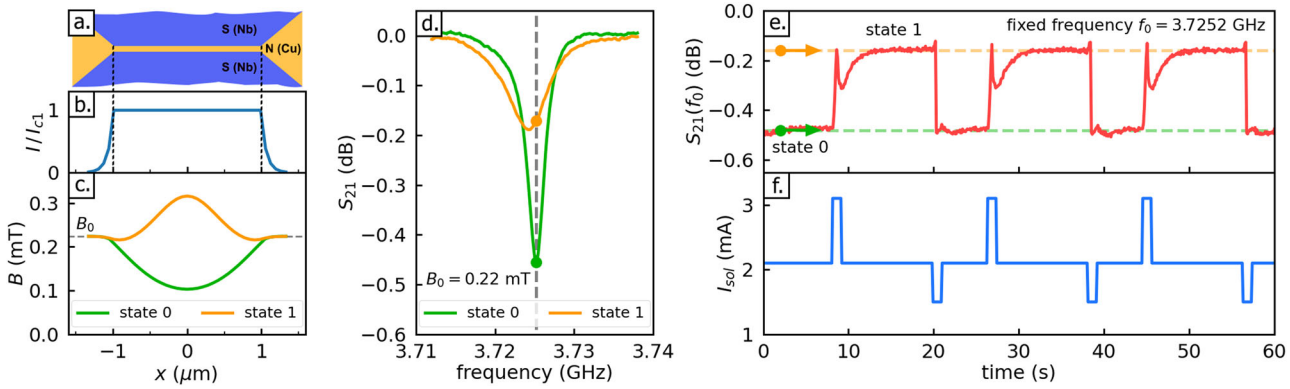

Fig. 3 | Switching between $N = 0$ and $N = 1$ Josephson vortex states. **a** Theoretically considered geometry of the sample; **b** considered distribution of the critical current density along the junction; **c** calculated distribution of the magnetic field inside the Josephson junction in the two states at the same external magnetic field $B_0 = 0.22$ mT inside the hysteresis region; **d** experimentally measured resonance peaks in the scattering parameter S_{21} at the same field; **e** experimental demonstration of the switching detection in S_{21} measured at a fixed frequency $f_0 = 3.7252$ GHz, shown in the image (**d**) by a vertical dashed line. Green and orange dots, arrows and dashed lines indicate the level of the signal from the resonator in two different states taken from the resonance peak measurements at frequency f_0 shown by the same dots in the image (**d**); **f** a series of current pulses applied to the solenoid to vary the magnetic field and switch between the two states (the long current pulse duration and relaxation time of the response are connected to the relaxation of the magnetic field in the solenoid, see the Experimental setup section in Methods for details).

local field distribution inside JJ is different: in $N = 0$ state, the external field is partially screened towards the junction center by Meissner currents (green line), while in $N = 1$ state the JV currents increase it (yellow line). Figure 3d shows the experimentally measured resonance curves corresponding to these two states, measured at the same field 0.22 mT. The resonant frequencies and quality factors clearly differ enabling a reliable distinguishing between them.

Switching between JV states

To demonstrate a possible working principle of the JV-based memory cell, we performed an experiment in which the switching between $N = 0$ and $N = 1$ states was driven by magnetic field. The results are presented in Fig. 3e, f. The current through the superconducting solenoid was first set to zero and then to the value corresponding to the field $B_0 = 0.22$ mT. At this "write zero" condition, the system is in $N = 0$ state. The signal $S_{21} \approx -0.5$ dB corresponds to a non-destructive "read" of "zero" state of the memory. Then, an additional current pulse of ~1 s duration was applied to temporarily increase the field and drive the JJ to $N = 1$ state. A single Josephson vortex penetrates the JJ and remains there when the field returns to B_0; this is "write one" operation. The signal S_{21} raises to ≈−0.2 dB; that corresponds to a non-destructive "read" of "one" state of the memory. Similarly, when negative current pulse is applied, the field decreases below the hysteresis region, the Josephson vortex exits the junction, and when the field returns back to the value B_0 the JJ remains in $N = 0$ state—"zero" state of the memory. The write/read processes are perfectly reproducible. This demonstrates the system to work indeed as a memory element. Note that in the experiment the used superconducting solenoid has a long relaxation time $\tau = L/R \sim 10^0$ s, due to a large inductance L of the solenoid and a low resistance R of the in-parallel connected "open" superconducting switch. That explains why the detection signal S_{21} does not change immediately but evolves in a seconds. Our model showed that in practice, the pulses required for successful write processes can be as short as ~40 ps, which enables a state-of-the art fast "write" operations[1]. In addition, we simulated the behavior of the system when two identical pulses are applied consecutively. The simulation results are presented in the Supplementary Note 2. We made sure that the system remains in the previous state when the pulse of the same type is repeated.

Discussion

Towards competitive JV-based memories

The main goals of the present work were to suggest a cryogenic memory cell based on a single Josephson vortex in SNS junctions, dress the microscopic picture of the JV dynamics and to demonstrate one of possible working principles of JV-based memory function. Nevertheless, the obtained experimental results already enable us to foresee several advantages of these memories and envisage some routes for the performance optimisation.

Currently, cryogenic microwave devices integrating JJ are actively developed, such as generators[63,64], amplifiers[65,66], tunable resonators[67–69] or impedances[70]. With this respect, the use of a similar technology and signal transmission method in the present work is advantageous as it makes our JV-based memories on-chip compatible with the existing rich family of superconducting microwave devices. Furthermore, the results of the present work open promising options for the development of advantageous quantum-classical digital/analogue interfaces for quantum computers. Indeed, the transmission of the microwave signals that control the quantum core, with its simultaneous noise isolation, is a bottleneck that is currently seen as the main challenge to further progress in increasing the number of qubits in quantum processors. The classical control system should be placed in a fridge near the quantum core, and possess high speed and energy efficiency of its digital part[71], while being easily compatible with the microwave part of electronics communicating with qubits. The proposed memory is exactly what is desired, since it can directly affect the microwave characteristics of analogue devices while being controlled by digital single-flux-quantum (SFQ) circuits[1,2], where the information is presented as JVs. This compatibility can be also highly sought after in hybrid digital/analogue implementations of superconducting neural networks[72].

The ability to encode several JV states at once is also advantageous as makes it possible to envisage other devices such as multi-bit memories, registers or counters[73–75]. Also, the use of artificial uniformity suggested in Fig. 3a enables a spatial localization of the vortex position. In principle, this could allow one to access the state of a specific bit. In addition, already in the studied simple linear JJ geometry, anti-vortices (JVs of the opposite flux direction) can also be used, thus forming basic elements of ternary logic, with '−1', '0' and '1' encoded states.

The speed of write/read operations and related energy dissipation are important parameters of cryogenic memories. In the experiment, the "write" pulse duration was very long, about ~1 s, because of a very large solenoid used. Though, in realistic memory elements, the JJ could be driven locally by a tiny current loop; the pulse duration could quite easily be reduced to $\sim 10^{-9}$ s, at least. The energy dissipated in the JJ upon "write" process is that required to put (remove) a single JV in (from) the JJ; it depends on JJ characteristics and can be estimated in the framework of our numerical model; for the studied JJs one gets ~1 aJ. The "read" process at resonance requires a time $\sim Q_l \times T$, where T is the period of the microwave excitation. For the studied (non-optimized) device one gets $\sim 10^{-7}$ s, which is

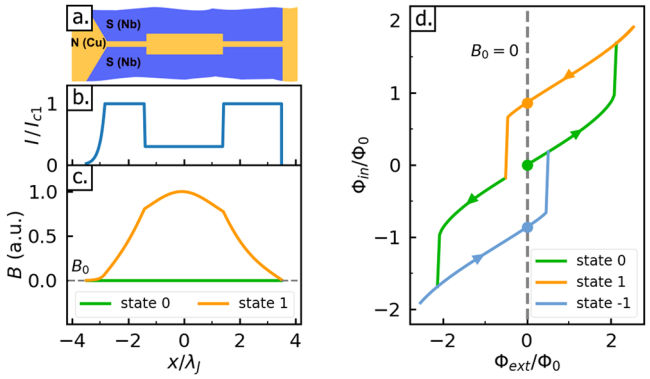

Fig. 4 | Suggestion for the memory element working at zero-magnetic field. a Top view of the junction; **b** the width modulation leads to a non-uniform distribution of the critical current density; **c** distribution of the magnetic field inside the junction at zero-external field for $N = 0$ state (green line) and $N = 1$ state (yellow line); **d** dependence of the total magnetic flux through the junction as a function of the external magnetic flux is hysteretic. Due to the peculiar geometry of the Josephson junction, the hysteresis region $0 \rightleftarrows \pm 1$ includes $\Phi_{ext} = 0$ (vertical dashed line).

quite long. Though, "read" operation is much less dissipative than "write" one, since the shaking microwave current and R_L are well below I_c and R_N. As a result, the total energy dissipated in the JJ during one "read" operation remains far below 1 aJ.

Evidently, at this early stage of development, the studied device was not optimized for serving as a JV-based memory element. Hereafter we list some ideas for improvements in the future. First, the write time can be reduced. Clearly, using large solenoids is not appropriate. Instead, tiny local superconducting loops could be designed for JV manipulation. Also, increasing the critical voltage V_c of the junction could be interesting. The speed of processes in SNS is determined by the critical frequency f_c, which is proportional to V_c. Our sample was far from the maximum possible value that can reach several mV[76]. In this way, the writing times can be reduced to ~10 ps.

Secondly, the size of the memory cell can be significantly reduced by using a different technology for the reading resonator. In this paper and in many works on superconducting quantum circuits, coplanar resonators are used due to the simplicity of their fabrication. However, recently there has been an increasing interest in finding ways to miniaturize them. One way is to use lumped-element resonators[77], the lateral size of which is already less than 200 microns at a frequency of 7 GHz and this is not the limit. Moreover, desired increase in the reading frequency will also lead to a further reduction in the size of the resonators.

Third, the difference in the detection signal S_{21} corresponding to the two states can be increased enabling their easier identification. This can be done by increasing the absorption of the resonator, according to the expression (1). For example, if our system had the internal Q-factor $Q_i = 5 \times 10^4$, the difference in output power would be 84%. Note that the values of Q_i and Q_c can be greatly varied in microwave coplanar resonators and reach values of the order of 10^6 [78]. However, large Q-factors would lead to long relaxations of the signal in the resonator. Therefore, the optimisation is necessary, depending on a specific use of the memory.

Finally, it would be interesting to avoid applying a permanent non-zero working field B_0. This cannot be achieved in standard long JJs because, according to the works[40,41], in JJs of a finite length there are no quasi-equilibrium states at a zero-field. For $0 \rightleftarrows 1$ hysteresis to occur around zero-field, it is necessary to artificially strengthen the barriers for the JV entry. This can be done, for example, by increasing the density of the critical current at the edges of the junction. Figure 4a suggests a sketch of such a junction which is narrower at its ends and wider in the center. Numerical simulations of such a junction take into account a non-uniform critical current density distribution, Fig. 4b. They show that such a JJ indeed enables $+1$ and -1 quasi-equilibrium JV states at a zero-field along with the true equilibrium state 0 with no magnetic field inside the junction. The local field distribution in these states is shown in Fig. 4c. The full hysteresis curve of such a junction upon external field cycling is shown in Fig. 4d. Now, the working field can be selected equal to zero (vertical dashed line). In addition, it would be interesting to explore the suggestion[79] of generating JVs states by purely electric means.

Conclusion

To conclude, we presented a cryogenic memory cell in which the information is encoded in an individual Josephson vortex present in a long Superconductor/Normal metal/Superconductor Josephson junction. The junction is embedded into the superconducting coplanar resonator and thus is directly compatible with the state of the art cryogenic microwave technology. The desired number of vortices in the junction is set by applying pulses of magnetic field; an energy-efficient non-destructive readout is done by slightly shaking the introduced vortices with a weak microwave excitation (two orders of magnitude below the critical current), and by measuring the microwave response of the resonator. The process is similar to the matchbox shaking and sound listening—a common way to know if there are matches inside with no need for box opening. We make the first assessment of the memory performance and suggest different routes for its improvement. While for now only 0 and 1 vortex states were exploited to demonstrate a standard memory function, it is straightforward to create multi-state memories and more complex logic elements by making longer Josephson junctions, by tuning material's properties and shaping the device geometry.

Methods

Device fabrication

The device consists of four identical Nb/Cu/Nb junctions integrated into coplanar microwave resonators of different resonant frequencies. The resonators are notch-coupled to the common coplanar waveguide. The lateral size of the whole device is ≈ 9 mm. To realize it, Nb/Cu films were first deposited onto a highly resistive silicon wafer by successive magnetron sputtering of 50 nm copper (bottom layer) and 100 nm niobium (top layer). Then, coplanar structures were fabricated using etching through the resist mask. Niobium was removed by Reactive Ion Etching in $CF_4 + O_2$ plasma; copper—using wet chemical solution $FeCl_3$. The superconducting critical temperature of the Nb/Cu bilayer, $T_c = 8.25$ K, was measured by four-terminal electron transport method.

Experimental setup

In the experiments, the resonators were excited and probed individually at their resonant frequencies (3–5 GHz) using two microwave lines connected to the device. The input line contained several cryogenic attenuators with a total attenuation of −60 dB. The output line was equipped with a cryogenic amplifier with a gain of +40 dB. The parameter S_{21} was measured using a vector network analyzer (VNA). The measurements were provided in a dilution refrigerator at a base temperature of 35 mK. A superconducting solenoid was used to create an external magnetic field, with a field to current conversion constant $B/I_{sol} = 0.1068$ T/A. The solenoid with inductance $L \approx 20$ H is shunted by a persistent switcher with resistivity $R \approx 20$ Ω. Therefore the magnetic field relaxes to a new value with the characteristic time $\tau = L/R \approx 1s$.

Numerical model

A distributed model of a long contact was used similarly to the work[62] (see the Supplementary Note 1 for more details). The gate-like distribution of the critical current was considered, as shown in Fig. 3b. For the calculations, the junction was divided in 30 segments in its central part, with the same critical current $I_{c1} = 32.49\ \mu A$ in each segment; the JJ edges were divided in 5 segments each, with exponentially decaying critical current. The normalized JJ length was taken $L/\lambda_J^{fit} = 4.09$. For the complex impedance calculations, a weak harmonic excitation current was used, $I/I_{c1} = 0.01\sin(0.01\tau)$. As for the voltage across the junction, we took the half-sum of the derivatives of the superconducting phases at the edges of the junction, $V/V_c = 0.5(\dot{\varphi}_1 + \dot{\varphi}_{30})$. Then we calculated the JJ impedance and used expressions (2) to obtain the resonators parameters f_r and Q_i.

Data availability

All relevant data are available from the corresponding authors upon reasonable request.

Received: 10 August 2023; Accepted: 21 February 2024;
Published online: 11 March 2024

References

1. Cuthbert, M. et al. International roadmap for devices and systems. Cryogenic electronics and quantum information processing. 2022 Edition (IEEE, 2022).
2. Likharev, K. K. & Semenov, V. K. RSFQ logic/memory family: a new Josephson-junction technology for sub-terahertz-clock-frequency digital systems. *IEEE Trans. Appl. Supercond.* **1**, 3–28 (1991).
3. Holmes, D. S., Ripple, A. L. & Manheimer, M. A. Energy-efficient superconducting computing-power budgets and requirements. *IEEE Trans. Appl. Supercond.* **23**, 1701610 (2013).
4. Soloviev, I. I. et al. Beyond Moore's technologies: operation principles of a superconductor alternative. *Beilstein J. Nanotechnol.* **8**, 2689–2710 (2017).
5. Ying, L. et al. Development of multi-layer fabrication process for SFQ large scale integrated digital circuits. *IEEE Trans. Appl. Supercond.* **31**, 1–4 (2021).
6. Tolpygo, S. K. et al. Progress toward superconductor electronics fabrication process with planarized NbN and NbN/Nb layers. *IEEE Trans. Appl. Supercond.* **33**, 1–12 (2023).
7. Tanaka, M., Sato, R., Fujimaki, A., Takagi, K. & Takagi, N. Execution of stored programs by a rapid single-flux-quantum random-access-memoryembedded bit-serial microprocessor using 50-GHz clock frequency. *Appl. Phys. Lett.* **122**, 192601 (2023).
8. Ladd, T. D. et al. Quantum computers. *Nature* **464**, 45–53 (2010).
9. Devoret, M. H. & Schoelkopf, R. J. Superconducting circuits for quantum information: an outlook. *Science* **339**, 1169–1174 (2013).
10. Soloviev, I. I., Klenov, N. V., Bakurskiy, S. V., Pankratov, A. L. & Kuzmin, L. S. Symmetrical Josephson vortex interferometer as an advanced ballistic single-shot detector. *Appl. Phys. Lett.* **105**, 202602 (2014).
11. Krantz, P. et al. A quantum engineer's guide to superconducting qubits. *Appl. Phys. Rev.* **6**, 021318 (2019).
12. Kjaergaard, M. et al. Superconducting qubits: current state of play. *Annu. Rev. Condens. Matter Phys.* **11**, 369–395 (2020).
13. Arute, F. et al. Quantum supremacy using a programmable superconducting processor. *Nature* **574**, 505–510 (2019).
14. Vozhakov, V. A. et al. State control in superconducting quantum processors. *Phys. Usp.* **65**, 421–439 (2022).
15. Soloviev, I. I. et al. Adiabatic superconducting artificial neural network: basic cells. *J. Appl. Phys.* **124**, 152113 (2018).
16. Klenov, N. V., Schegolev, A. E., Soloviev, I. I., Bakurskiy, S. V. & Tereshonok, M. V. Energy efficient superconducting neural networks for high-speed intellectual data processing systems. *IEEE Trans. Appl. Supercond.* **28**, 1301006 (2018).
17. Ishida, K. et al. Superconductor computing for neural networks. *IEEE Micro* **41**, 19–26 (2021).
18. Semenov, V. K., Golden, E. B. & Tolpygo, S. K. A new family of bioSFQ logic/memory cells. *IEEE Trans. Appl. Supercond.* **32**, 1–5 (2022).
19. Skryabina, O. V. et al. Superconducting bio-inspired Au-nanowire-based neurons. *Nanomaterials* **12**, 1671 (2022).
20. Schneider, M. et al. SuperMind: a survey of the potential of superconducting electronics for neuromorphic computing. *Supercond. Sci. Technol.* **35**, 053001 (2022).
21. Yamauchi, T., San, H., Yoshikawa, N. & Chen, O. Design and implementation of energy-efficient binary neural networks using adiabatic quantum-flux-parametron logic. *IEEE Trans. Appl. Supercond.* **33**, 1–5 (2023).
22. Nagasawa, S., Hinode, K., Satoh, T., Kitagawa, Y. & Hidaka, M. Design of all-dc-powered high-speed single flux quantum random access memory based on a pipeline structure for memory cell arrays. *Supercond. Sci. Technol.* **19**, S325 (2006).
23. Semenov, V. K., Polyakov, Y. A. & Tolpygo, S. K. Very large scale integration of Josephson-junction-based superconductor random access memories. *IEEE Trans. Appl. Supercond.* **29**, 1–9 (2019).
24. Takeshita, Y. et al. High-speed memory driven by SFQ pulses based on 0-π SQUID. *IEEE Trans. Appl. Supercond.* **31**, 1–6 (2021).
25. Ligato, N., Strambini, E., Paolucci, F. & Giazotto, F. Preliminary demonstration of a persistent Josephson phase-slip memory cell with topological protection. *Nat. Commun.* **12**, 5200 (2021).
26. Larkin, T. I. et al. Ferromagnetic Josephson switching device with high characteristic voltage. *Appl. Phys. Lett.* **100**, 222601 (2012).
27. Goldobin, E. et al. Memory cell based on a φ Josephson junction. *Appl. Phys. Lett.* **102**, 242602 (2013).
28. Baek, B., Rippard, W. H., Benz, S. P., Russek, S. E. & Dresselhaus, P. D. Hybrid superconducting-magnetic memory device using competing order parameters. *Nat. Commun.* **5**, 3888 (2014).
29. Niedzielski, B. M., Gingrich, E. C., Loloee, R., Pratt, W. P. & Birge, N. O. S/F/S Josephson junctions with single-domain ferromagnets for memory applications. *Supercond. Sci. Technol.* **28**, 085012 (2015).
30. Bakurskiy, S. V. et al. Protected 0-π states in SIsFS junctions for Josephson memory and logic. *Appl. Phys. Lett.* **113**, 082602 (2018).
31. Dayton, I. M. et al. Experimental demonstration of a Josephson magnetic memory cell with a programmable π-junction. *IEEE Magn. Lett.* **9**, 1–5 (2018).
32. Suleiman, M., Sarott, M. F., Trassin, M., Badarne, M. & Ivry, Y. Nonvolatile voltage-tunable ferroelectric-superconducting quantum interference memory devices. *Appl. Phys. Lett.* **119**, 112601 (2021).
33. Golod, T., Iovan, A. & Krasnov, V. M. Single Abrikosov vortices as quantized information bits. *Nat. Commun.* **6**, 8628 (2015).
34. Golod, T., Morlet-Decarnin, L. & Krasnov, V. Word and bit line operation of a 1 × 1μm superconducting vortex-based memory. *Nat. Commun.* **14**, 4926 (2023).
35. Guarcello, C., Solinas, P., Di Ventra, M. & Giazotto, F. Solitonic Josephson-based meminductive systems. *Sci. Rep.* **7**, 46736 (2017).
36. Barone, A. & Paterno, G. *Physics and Applications of the Josephson Effect*. (John Wiley & Sons, New York, 1982).
37. Ustinov, A. Solitons in Josephson junctions. *Phys. D: Nonlinear Phenom.* **123**, 315–329 (1998).
38. Owen, C. S. & Scalapino, D. J. Vortex structure and critical currents in Josephson junctions. *Phys. Rev.* **164**, 538–544 (1967).
39. Pagano, S., Ruggiero, B. & Sarnelli, E. Magnetic-field dependence of the critical current in long Josephson junctions. *Phys. Rev. B* **43**, 5364–5369 (1991).
40. Kuplevakhsky, S. V. & Glukhov, A. M. Static solitons of the sine-Gordon equation and equilibrium vortex structure in Josephson junctions. *Phys. Rev. B* **73**, 024513 (2006).
41. Kuplevakhsky, S. V. & Glukhov, A. M. Exact analytical solution of a classical Josephson tunnel junction problem. *Low. Temp. Phys.* **36**, 1012–1021 (2010).
42. Cirillo, M., Grønbech-Jensen, N., Samuelsen, M. R., Salerno, M. & Rinati, G. V. Fiske modes and Eck steps in long Josephson junctions: theory and experiments. *Phys. Rev. B* **58**, 12377 (1998).
43. Grønbech-Jensen, N., Lomdahl, P. & Samuelsen, M. Phase-locking of long annular Josephson junctions coupled to an external rf magnetic field. *Phys. Lett. A* **154**, 14–18 (1991).
44. Grønbech-Jensen, N., Malomed, B. A. & Samuelsen, M. R. Dynamics of an annular Josephson junction in a rotating magnetic field. *Phys. Rev. B* **46**, 294–300 (1992).
45. Wallraff, A. et al. Quantum dynamics of a single vortex. *Nature* **425**, 155–158 (2003).
46. Golovchanskiy, I. A. et al. Ferromagnetic resonance with long Josephson junction. *Supercond. Sci. Technol.* **30**, 054005 (2017).

47. Josephson, B. D. Supercurrents through barriers. *Adv. Phys.* **14**, 419–451 (1965).
48. Bean, C. & Livingston, J. Surface barrier in type-II superconductors. *Phys. Rev. Lett.* **12**, 14 (1964).
49. Saint-James, D., Sarma, G. & Thomas, E. *Type II Superconductivity* (Elsevier Science & Technology, 1969).
50. Tinkham, M. *Introduction to Superconductivity: Second Edition* (Dover Publications, 2004).
51. Schmidt, V. *The Physics of Superconductors: Introduction to Fundamentals and Applications* (Springer Berlin Heidelberg, 2013).
52. Kupriyanov, M. Y. & Likharev, K. K. Effect of edge barrier on critical current in superconducting film. *Fizika Tverdogo Tela* **16**, 2829–2833 (1974). [*Sov. Phys.-Solid State* **16**, 1835-1837 (1975)].
53. Zeldov, E. et al. Geometrical barriers in high-temperature superconductors. *Phys. Rev. Lett.* **73**, 1428–1431 (1994).
54. Ooi, S., Mochiku, T. & Hirata, K. Periodic oscillations of Josephson-vortex flow resistance in $Bi_2Sr_2CaCu_2O_{8+y}$. *Phys. Rev. Lett.* **89**, 247002 (2002).
55. Moll, P. J., Zhu, X., Cheng, P., Wen, H.-H. & Batlogg, B. Intrinsic Josephson junctions in the iron-based multi-band superconductor $(V_2Sr_4O_6)Fe_2As_2$. *Nat. Phys.* **10**, 644–647 (2014).
56. Probst, S., Song, F. B., Bushev, P. A., Ustinov, A. V. & Weides, M. Efficient and robust analysis of complex scattering data under noise in microwave resonators. *Rev. Sci. Instrum.* **86**, 024706 (2015).
57. Gao, J. The physics of superconducting microwave resonators. Ph.D. thesis, California Institute of Technology (2008).
58. Zhai, Z., Parimi, P. V. & Sridhar, S. Nonlinear microwave impedance of short and long Josephson junctions. *Phys. Rev. B* **59**, 9573–9580 (1999).
59. Dremov, V. V. et al. Local Josephson vortex generation and manipulation with a magnetic force microscope. *Nat. Commun.* **10**, 1–9 (2019).
60. Grebenchuk, S. Y. et al. Observation of interacting Josephson vortex chains by magnetic force microscopy. *Phys. Rev. Res.* **2**, 023105 (2020).
61. Hovhannisyan, R. A., Grebenchuk, S. Y., Baranov, D. S., Roditchev, D. & Stolyarov, V. S. Lateral Josephson junctions as sensors for magnetic microscopy at nanoscale. *J. Phys. Chem. Lett.* **12**, 12196–12201 (2021).
62. Stolyarov, V. S. et al. Revealing Josephson vortex dynamics in proximity junctions below critical current. *Nano Lett.* **22**, 5715–5722 (2022).
63. Cassidy, M. C. et al. Demonstration of an ac Josephson junction laser. *Science* **355**, 939–942 (2017).
64. Yan, C. et al. A low-noise on-chip coherent microwave source. *Nat. Electron.* **4**, 885–892 (2021).
65. Macklin, C. et al. A near–quantum-limited Josephson traveling-wave parametric amplifier. *Science* **350**, 307–310 (2015).
66. Sivak, V., Shankar, S., Liu, G., Aumentado, J. & Devoret, M. Josephson array-mode parametric amplifier. *Phys. Rev. Appl.* **13**, 024014 (2020).
67. Palacios-Laloy, A. et al. Tunable resonators for quantum circuits. *J. Low. Temp. Phys.* **151**, 1034–1042 (2008).
68. Kennedy, O. et al. Tunable Nb superconducting resonator based on a constriction nano-SQUID fabricated with a Ne focused ion beam. *Phys. Rev. Appl.* **11**, 014006 (2019).
69. Strickland, W. M. et al. Superconducting resonators with voltage-controlled frequency and nonlinearity. *Phys. Rev. Appl.* **19**, 034021 (2023).
70. Habib, Y. M. et al. Measurements and modeling of the microwave impedance in high-T_c grain-boundary Josephson junctions: fluxon generation and rf Josephson-vortex dynamics. *Phys. Rev. B* **57**, 13833–13844 (1998).
71. McDermott, R. et al. Quantum-classical interface based on single flux quantum digital logic. *Quantum Sci. Technol.* **3**, 024004 (2018).
72. Islam, M. M., Alam, S., Hossain, M. S., Roy, K. & Aziz, A. A review of cryogenic neuromorphic hardware. *J. Appl. Phys.* **133**, 070701 (2023).
73. Fujiwara, K., Hoshina, H., Koshiyama, J. & Yoshikawa, N. Design and component test of RSFQ packet decoders for shift register memories. *Phys. C* **378-381**, 1475–1480 (2002).
74. Katam, N. K., Zha, H., Pedram, M. & Annavaram, M. Multi fluxon storage and its implications for microprocessor design. *J. Phys. Conf. Ser.* **1559**, 012004 (2020).
75. Jardine, M. A. & Fourie, C. J. Hybrid RSFQ-QFP superconducting neuron. *IEEE Trans. Appl. Supercond.* **33**, 1302409 (2023).
76. Soloviev, I. et al. Miniaturization of Josephson junctions for digital superconducting circuits. *Phys. Rev. Appl.* **16**, 044060 (2021).
77. Zotova, J. et al. Compact superconducting microwave resonators based on Al-AlO_x-Al capacitors. *Phys. Rev. Appl.* **19**, 044067 (2023).
78. Verjauw, J. et al. Investigation of microwave loss induced by oxide regrowth in high-Q niobium resonators. *Phys. Rev. Appl.* **16**, 014018 (2021).
79. Roditchev, D. et al. Direct observation of Josephson vortex cores. *Nat. Phys.* **11**, 332 (2015).

Acknowledgements

The authors are grateful to O.V. Skryabina for useful discussions of the obtained results and assistance in the experimental studies. The authors are grateful to MIPT Collective Use Center for providing facilities for samples fabrication. The sample preparation process was supported by the Ministry of Science and Higher Education of the Russian Federation (No. FSMG-2023-0014). The experiments were carried out with the support of the Russian Science Foundation, Grant No. 23-72-30004 (https://rscf.ru/project/23-72-30004/). The theoretical modeling of high-frequency spectroscopy of the Josephson vortex dynamics and switching effects was supported by the Russian Science Foundation, Grant No. 20-12-00130 (https://rscf.ru/project/20-12-00130/). The concept of cryogenic memory was developed with the financial support of the Strategic Academic Leadership Programme "Priority-2030" (NUST MISIS Grant No. K2-2022-029) and French project CrysTop (ANR-19-CE30-0034).

Author contributions

V.S.S. suggested the idea of the experiment and conceived the project; D.S.K., I.A.G., and V.S.S. organized and supervised the experiments and sample design; D.S.K., A.G.S., I.A.G., and V.S.S. fabricated the samples; D.S.K. carried out all microwave cryogenic measurements and collected the data; D.S.K., V.I.R., I.I.S., M.Yu.K., and V.S.S. carried out numerical calculations and adapted the parameters for the experiment data approximation; D.S.K., V.I.R., I.I.S., D.R., and V.S.S. wrote the manuscript with contributions from all authors.

Competing interests

The authors declare no competing interests.

Additional information

Supplementary information The online version contains supplementary material available at https://doi.org/10.1038/s42005-024-01570-4.

Correspondence and requests for materials should be addressed to Dmitrii S. Kalashnikov or Vasily S. Stolyarov.

Peer review information *Communications Physics* thanks the anonymous reviewers for their contribution to the peer review of this work.